 doi:10.20944/preprints202011.0574.v1

Article

Application of Reflectance Ratios on High-Resolution Satellite Imagery to Remotely Identify Eucalypt Vegetation

Kelsee Baranowski [1], Teairah Taylor [2], Brian Lambert[1], and Nita Bharti[1,*]

[1] Department of Biology, Center for Infectious Disease Dynamics, The Pennsylvania State University, University Park, PA
[2] Department of Communication, Cornell University, Ithaca, NY
* Correspondence: ktb5143@psu.edu, nita@psu.edu

The scale and accessibility of passive global surveillance have rapidly increased over time. This provides an opportunity to calibrate the performance of models, algorithms, and reflectance ratios between remote sensing devices. Here we test the sensitivity and specificity of Eucalypt chlorophyll-*a* reflectance ratio (ECARR) and Eucalypt chlorophyll-*b* reflectance ratio (ECBRR) to remotely identify eucalypt vegetation in Queensland, Australia. We compare reflectance ratio values from Sentinel-2 and Planet imagery across four sites of known vegetation composition. All imagery was transformed to reflectance values and Planet imagery was additionally scaled to harmonize across Planet Scenes. ECARR can identify eucalypt vegetation remotely with high sensitivity, but shows low specificity and is impacted by the density of the vegetation. ECBRR reflectance ratios show similar sensitivity and specificity when identifying eucalypt vegetation but with values an order of magnitude smaller than ECARR. We find that ECARR was better at identifying eucalypt vegetation in the Sentinel-2 imagery than Planet imagery. ECARR can serve as a general chlorophyll indicator but is not a specific index to identify *Eucalyptus* vegetation with certainty.

Keywords: Eucalypt chlorophyll-*a* reflectance ratio; Eucalypt chlorophyll-*b* reflectance ratio; vegetation identification; Sentinel-2; Planet Dove

1. Introduction

Vegetation communities with greater biodiversity offer benefits for ecosystem services, resilience against degradation, food security, drug development, and natural sustainability of habitats [1–3]. However, the strength created by mixed communities can also lead to challenges for categorizing the extent of individual species and the management of vulnerable species in these ecosystems. Knowing the location and extent of individual species' ranges can aid in the conservation and survival of key species. To inform targeted management of woody vegetation species vulnerable to pests, plant pathogens, and invasive species, it is critical to know the locations and connectivity of susceptible hosts [4,5]. Likewise, as climate change affects rainfall, temperature, and atmospheric CO_2 levels, identifying where species already exist at the edge of their tolerances will aid in conservation of these species against local extinctions [6,7]. Ground-level approaches would require years of data collection to amass this knowledge, so many researchers look to remote sensing techniques and modeling to identify species distributions across the landscape.

Modeling approaches often estimate species extent with population viability analyses [8], species distribution modeling, or dynamic range models [9]. Each model uses various biotic

 doi:10.20944/preprints202011.0574.v1

and abiotic factors important for the species' phenology but all of these models require some data parameter that relates to the known occurrences of the species. Some remote sensing platforms have been successful in mapping vegetation distributions, such as the Queensland Herbarium's Vegetation Management Regional Ecosystem (VMRE) mapping series. This series leverages remote sensing data with ground surveys and environmental maps to show bi-annual vegetation dynamics from 1997 to the present in Queensland, Australia [10,11]. However, this dataset represents years of extensive work and effort on the ground to create its high-quality maps.

Remote sensing approaches alone have not been enough to identify species' distributions with certainty. Mixed vegetation communities muddle the spectral signal from an individual's species [12], so reflectance has not been characterized for many species. Multispectral vegetation indices, such as Normalized Difference Vegetation Index (NDVI) have been developed to gauge chlorophyll properties of vegetation remotely, but do not provide species-specific information. NDVI utilizes the difference in reflectance of light between the red and near-infrared (NIR) channels to provide a proxy for the vegetation's 'greenness' [13]. Most vegetation indices are general and identify chlorophyll broadly, but some have been developed to measure chlorophyll of specific types of vegetation.

Reflectance ratios were previously developed to remotely estimate the amount of chlorophyll-*a*, chlorophyll-*b*, chlorophyll-*a*+*b*, and total carotenoids in *Eucalyptus* leaves [14]. The correlation between chlorophyll content and the reflectance of single wavelengths of light was measured using a hand-held spectroradiometer. Two sets of algorithms were derived to estimate chlorophyll levels of *Eucalyptus* leaves, one based solely on reflectance values and one adjusted to account for different species and maturity of leaves [14].
Remote Estimation of Eucalypt Chlorophyll Algorithm:

$$\text{Eucalypt Chlorophyll-}a\text{ Reflectance Ratio (ECARR)} = 0.0161 \times [\![{}^{\dagger}R672 / (R550 \times R708)]\!]\text{^}0.7784 \quad (1)$$

$$\text{Eucalypt Chlorophyll-}b\text{ Reflectance Ratio (ECBRR)} = 0.0337 \times [\![R672 / R550]\!]\text{ ^}1.8695 \quad (2)$$

[†]Where R represents the reflectance value at that wavelength of light.

Remote Estimation of Eucalypt Chlorophyll Scatter Adjusted Algorithm:

$$\text{Eucalypt Chlorophyll-}a\text{ Reflectance Ratio} = 0.0008 \times [\![R860 / (R550 \times R708)]\!]\text{^}1.2403 \quad (3)$$

$$\text{Eucalypt Chlorophyll-}b\text{ Reflectance Ratio} = 0.00005 \times [\![R860 / R550]\!]\text{^}3.5168 \quad (4)$$

These algorithms have been applied by others on imagery collected by different sensors [15–17] but each of these studies had limitations. Coops et al.,[15] showed a weak correlation using a modified index [18] to estimate chlorophyll-*a* on general eucalypt species but showed stronger correlations on individual species rather than mixed-species stands. Giles et al. [19] used Eucalypt chlorophyll-*a* reflectance ratio (ECARR) values from MODIS MCDA434A imagery as a model parameter. These images have a moderate spatial resolution (500m) and the spectral bands do not closely match the correlated wavelengths in the original algorithm in which they applied Equation (1).

 doi:10.20944/preprints202011.0574.v1

Few datasets with the quality and detail of the Queensland VMRE are maintained and updated. However, leveraging the vast amount of passive global surveillance could help increase the availability of these types of data. Applying these methods would be particularly beneficial in areas where vegetation classification and extent are not documented in a detailed, systematic way. This approach could also improve our understanding of vegetation dynamics and changing biodiversity due to the longitudinal time range of satellites. Here, we test the application of the scatter adjusted Eucalypt chlorophyll-*a* reflectance ratio Equation (3) and Eucalypt chlorophyll-*b* reflectance ratio Equation (4) on three different vegetation communities. Using high-resolution satellite imagery from Planet and Sentinel-2, we test the sensitivity and specificity of these reflectance ratios to remotely identify areas of known vegetation composition in Queensland, Australia.

Satellite Selection

We compared data on spectral bands, spatial resolution, and capture rates from several satellite sensors for the closest possible match to the original algorithm developed by Datt [14]. Due to the physical constraints of the sensor and trade-off between spectral and spatial resolutions [20], satellites aggregate information from ranges of the electromagnetic spectrum into a single band. Therefore, it's not always possible to isolate reflectance values at a precise wavelength. Therefore, satellites with spectral bands that centered wavelengths close to the reflectance values with high correlations were used. By comparing 12 different satellite sensor types, we identified Planet and Sentinel-2 products that collected bands with center wavelengths proximal to the reflectance values in the scatter adjusted algorithms Equation (3) and Equation (4).

Sentinel-2, available beginning in 2015, collects data across thirteen spectral bands with a resolution of 10-60m. Two different instruments collect imagery, the Sentinel-2A and Sentinel-2B [21]. The central wavelengths of both instruments are within 1 nanometer of each other (Table 2), so both instrument types were used for analyses. Planet Doves collect nearly daily imagery of the globe with 3-meter resolution across four bands, red, green, blue, and near-infrared [22] (Table 1). They collect data with two different types of satellites, one PS2 sensor with a "2-stripe" filter separating the red, green, and blue channels from the NIR channel and the other a PS2.SD sensor with a butcher block style filter, where the four channels are stacked [23]. The PS2.SD sensor has been collecting data since 2019. We chose the PS2.SD sensor for this analysis due to the range of the NIR spectral band, whose center wavelength more closely matched the R860 value in the scatter adjusted algorithm Equation (3) and Equation (4). Additionally, this sensor matches more closely with and is interoperable with Sentinel-2 imagery [23].

Table 1. Sentinel-2A and Sentinel-2B instrument spectral band description [21].

Band	Center Wavelength (nm) Sentinel-2A	Center Wavelength (nm) Sentinel-2B	Spatial Resolution
Band 3	559.8	559.0	10m
Band 4	664.6	664.9	10m
Band 5	704.1	703.8	10m
Band 8	832.8	832.9	10m
Band 8A	864.7	864	20m

Preprints (www.preprints.org) | NOT PEER-REVIEWED | Posted: 23 November 2020 doi:10.20944/preprints202011.0574.v1

Table 2. Planet PS2.SD instrument spectral band description [23].

Band	Spectral Range (nm)	Approximate Center Wavelength (nm)	Spatial Resolution
Band 1	464-517	490	3m
Band 2	547-585	566	3m
Band 3	650-682	666	3m
Band 4	846-888	867	3m

Area of study

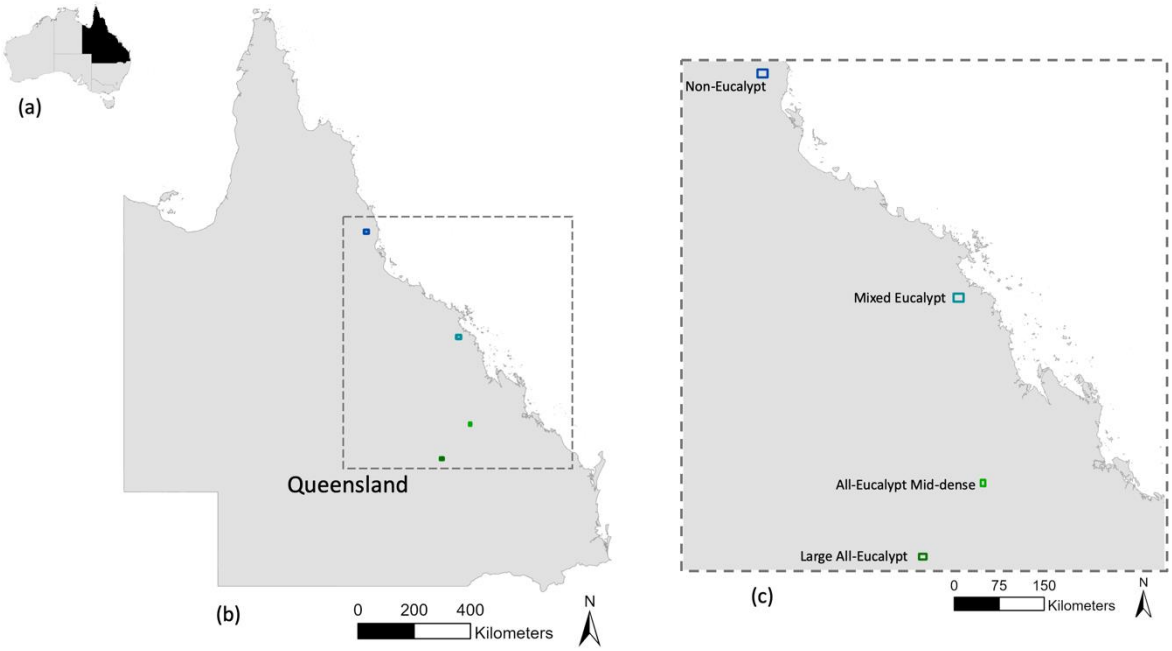

Figure 1. Map of study sites in Queensland, Australia. (a) Australia (grey) showing the state Queensland (black). (b) Queensland with selected vegetation sites, area of interest in box shown in (c). (c) Northeast coastal region of Queensland with selected vegetation sites.

We selected locations by first associating vegetation community information from the Regional Ecosystem Description Database with the 2017 Queensland Herbarium's Vegetation Management Regional Ecosystem (VMRE) map [11]. We chose four sites of different vegetation compositions and density structures (Figure 1). We compare two sites of all-eucalypt vegetation species, one site of mixed eucalypt and non-eucalypt vegetation, and one site of non-eucalypt vegetation species. We define eucalypt vegetation as species belonging to the tribe Eucalypteae. Three sites are between 105-108km^2 in size and contain protected areas where the vegetation communities are very likely to be the same composition in 2020 as described in the 2017 VMRE map [10]. The fourth site is an area 70 km^2 in size of mid-dense eucalypt vegetation. There are no comparable areas of dense or mid-dense all-eucalypt vegetation in the 2017 VMRE map.

The large all-eucalypt site is in Carnarvon National Park in southern Queensland and contains mostly sparse vegetation with areas of mid-dense vegetation commonly containing *Corymbia citriodora, Eucalyptus melliodora, E. melanophloia, E. laevopinea, and E. tereticornis*

(Figure 1c). We selected a second all-eucalypt site of higher density to account for the sparseness in the first all-eucalypt site. The second all-eucalypt site is in Blackdown Tableland National Park and contains mid-dense areas of *Eucalyptus sphaerocarpa, E. cloeziana, E. melanoleuca,* and various *Eucalyptus* and *Corymbia* species. The mixed eucalypt site is near Pelion State Forest in northeastern Queensland (Figure 1c). This site was chosen because it contains eucalypt vegetation, non-eucalypt vegetation, agricultural fields, and human settlement. The area contains sparse to dense vegetation with the eucalypt area containing species such as *Corymbia intermedia, E. platyphylla, E. resiniferia, E. tereticornis* amongst others in varying abundances and the non-eucalypt area contains evergreen to semi-evergreen notophyll, microphyll, and mesophyll vine forests with the agricultural fields and human settlements. The non-eucalypt site is in Wooroonooran National Park in northeast Queensland and is comprised of dense notophyll vine forests and mesophyll forests containing species such as *Araucaria bidwillii, Acacia celsa, Allocasuarina littoralis* with small non-vegetated areas. The South Johnstore River passes through this site and it contains a very small cleared area. VMRE map description of sites shown in Figures S1-S4, Table S1-S4.

2. Materials and Methods

We retrieved 13-band Sentinel-2 imagery courtesy of the U.S. Geological Survey through the USGS Earth Explorer [24] and 4-band Planet imagery from the Planet Explorer tool [25]. We selected imagery that had high coverage of the area of interest and less than 5% cloud cover from the Australian winter and late spring/summer months (Table 3) to assess seasonal variation patterns in detectability due to growth. The spring/summer imagery analysis was only performed on the three large sites. All Sentinel-2 imagery used was collected by Sentinel-2A instruments, except for the winter images of the all-eucalypt mid-dense and non-eucalypt site, which were collected by a Sentinel-2B instrument. A cloud-free Sentinel-2 image of the non-eucalypt site was not available in the winter of 2019, so an image from 2018 was used. Additionally, a full area coverage images of the non-eucalypt site in winter months and large all-eucalypt site in summer in Planet imagery was not available, as capture over these areas just began in June 2019. Therefore, we used images with 98% coverage of the area (Table 3). We processed all imagery using ESRI's ArcGIS Pro Version 2.5 [26] and analyzed all layers in the WGS84 UTM Zone 55S projection.

Table 3. Location of sites and imagery dates used for analysis. Bounding box coordinates of sites and imagery collection dates for each satellite type and season. *These images comprise 98% of the area of interest.

	Bounding Box Coordinates		Winter Imagery Date		Spring/Summer Imagery Date	
Site	**Upper Right Coordinate**	**Lower Left Coordinate**	**Planet PS2.SD**	**Sentinel-2**	**Planet PS2.SD**	**Sentinel-2**
Large All-Eucalypt	- 24.895, 148.193	- 24.980, 148.082	May 7, 2019	April 1, 2019	*November 15, 2019	January 1, 2019
All-Eucalypt	-23.786, 149.074	-23.880, 149.008	May 17, 2019	May 6, 2019		

Mid-dense Mixed Eucalypt	- 20.982, 148.759	- 21.072, 148.655	May 7, 2019	March 12, 2019	November 8, 2019	December 2, 2018
Non-Eucalypt	- 17.620, 145.800	- 17.704, 145.699	*July 24, 2019	June 13, 2018	October 16, 2019	November 10, 2019

Bands 3, 4, 5, 8, and 8A in the Sentinel-2 imagery were scaled by a factor of 0.0001 to convert pixel values to surface reflectance. Corrected bands 4 and 8 were used to calculate the NDVI values using Equation (5). Corrected bands 3, 5, and 8A were used to calculate ECARR and ECBRR with Equation (6) and Equation (7):

$$\text{NDVI} = (Band8 - Band4) / (Band8 + Band4) \quad (5)$$

$$\text{ECARR} = 0.0008 \times [\![\text{Band8A} / (\text{Band3} \times \text{Band5})]\!]\text{^}1.2403 \quad (6)$$

$$\text{ECBRR} = 0.00005 \times [\![\text{Band8A} / \text{Band3}]\!]\text{^}3.5168 \quad (7)$$

The resulting 20-meter resolution ECARR and ECBRR rasters were then clipped down to the area of interest and exported as a GEOTIFF. This process was repeated for the Sentinel-2 imagery at each site and each season. The spectral bands used in the NDVI calculations (Table 1) resulted in a 10-meter raster, which we resampled up to 20 meters for comparison to ECARR and ECBRR.

Bands 2, 3, and 4 in each Planet scene were individually multiplied by their respective Top of Atmosphere (TOA) reflectance coefficients and band coefficients to convert pixel value to TOA reflectance and harmonize the bands to other Planet scenes [23]. The TOA corrected bands 3 and 4 were then used to calculate NDVI to assess the area of living green vegetation using Equation (8). Corrected bands 2, 3, and 4 were used to calculate Eucalypt Chlorophyll-*a* Reflectance Ratio (ECARR) and Eucalypt Chlorophyll-*b* Reflectance Ratio (ECBRR) with Equation (9) and Equation (10).

$$\text{NDVI} = (Band4 - Band3)/(Band4 + Band3) \quad (8)$$

$$\text{ECARR} = 0.0008 \times [\![\text{Band4} / (\text{Band3} \times \text{Band2})]\!]\text{^}1.2403 \quad (9)$$

$$\text{ECBRR} = 0.00005 \times [\![\text{Band4} / \text{Band2}]\!]\text{^}3.5168 \quad (10)$$

The resulting 3-meter resolution raster was clipped down to the area of interest and exported as a GEOTIFF. This process was repeated for Planet imagery at each site and each season.

The resulting rasters from all sensors and seasons were then converted into points and intersected with the 2017 VMRE map of each site to associate pixel values with the related vegetation information. Pixel level results were visualized in R [27]. Values in areas of non-vegetation according to the 2017 VMRE map (i.e. rivers, cleared areas) were removed from the analysis. The results presented here are based on the winter imagery (Table 3). Late spring/summer imagery analysis shown in SI.

 doi:10.20944/preprints202011.0574.v1

3. Results

ECARR Results

ECARR values ranged between 0 and 1 across all sites and sensors (Table 4). Planet imagery had consistently higher ECARR values (site max: 0.708) than the Sentinel-2 imagery (site max: 0.264). The highest ECARR value was found in the mixed eucalypt site and the lowest values in the large all-eucalypt and non-eucalypt sites (Table 4). While eucalypt vegetation was positively identified in both all-eucalypt sites and the mixed eucalypt site (Figure 2a-c,e-g), it was also falsely detected in the non-eucalypt site (Figure 2d,h, Table 4). The Sentinel-2 data showed similar trends to Planet imagery with ECARR, but with narrower ranges of values. The narrowest range of values was found in the non-eucalypt site Sentinel-2 image, with the lowest maximum ECARR value of any site (Table 4).

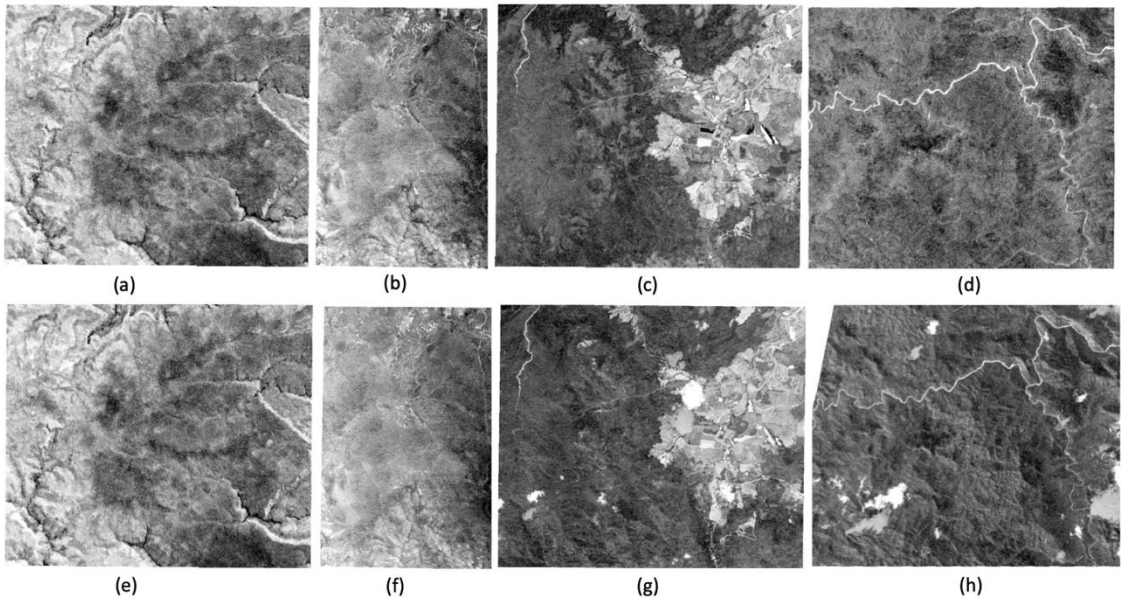

Figure 2. Results of Eucalypt Chlorophyll-a Reflectance Ratio (ECARR) calculations shown with a gradient scale from white (low) to black (high). Panels a-d) show Sentinel-2 imagery. Panels e-h) show Planet imagery. a) All-eucalypt site ECARR results Sentinel-2A imagery. b) All-eucalypt mid-dense site ECARR results Sentinel-2B imagery. c) Mixed eucalypt site ECARR results Sentinel-2A imagery. d) Non-eucalypt site ECARR results Sentinel-2B imagery. e) All-eucalypt site ECARR results Planet imagery. f) All-eucalypt mid-dense site ECARR results Planet imagery. g) Mixed eucalypt site ECARR results Planet imagery. h) Non-Eucalypt site ECARR results Planet imagery.

Table 4. Eucalypt Chlorophyll-*a* Reflectance Ratio value ranges and means of winter imagery for all sites and satellite sensors from winter imagery.

Satellite	ECARR Values	Large All-Eucalypt Site	All-Eucalypt Mid-dense Site	Mixed Eucalypt Site	Non-Eucalypt Site
Sentinel-2	Maximum	0.243	0.206	0.264	0.252
	Minimum	0.019	0.017	0.014	0.005
	Mean	0.077	0.094	0.148	0.140
Planet	Maximum	0.443	0.255	0.708	0.605
	Minimum	0.000	0.000	0.000	0.002
	Mean	0.160	0.108	0.321	0.271

Preprints (www.preprints.org) | NOT PEER-REVIEWED | Posted: 23 November 2020 doi:10.20944/preprints202011.0574.v1

Comparing ECARR values by vegetation type showed areas of non-eucalypt vegetation had higher mean values than areas of only eucalypts (Figure 3) and ANOVA tests show these differences in vegetation were significant (Table S7, S9) for both satellite types. Receiver Operating Characteristic (ROC) curves testing ECARRs sensitivity and specificity to classify eucalypt vegetation across sensors (Figure S5, S6) show the Sentinel-2 instrument was better at identifying eucalypt vegetation (AUC: 0.949, Accuracy: 0.904, PPV: 0.949, NPV: 0.862) than the Planet Dove (AUC: 0.906, Accuracy: 0.872, PPV: 0.897, NPV: 0.846) (Table S5, S6).

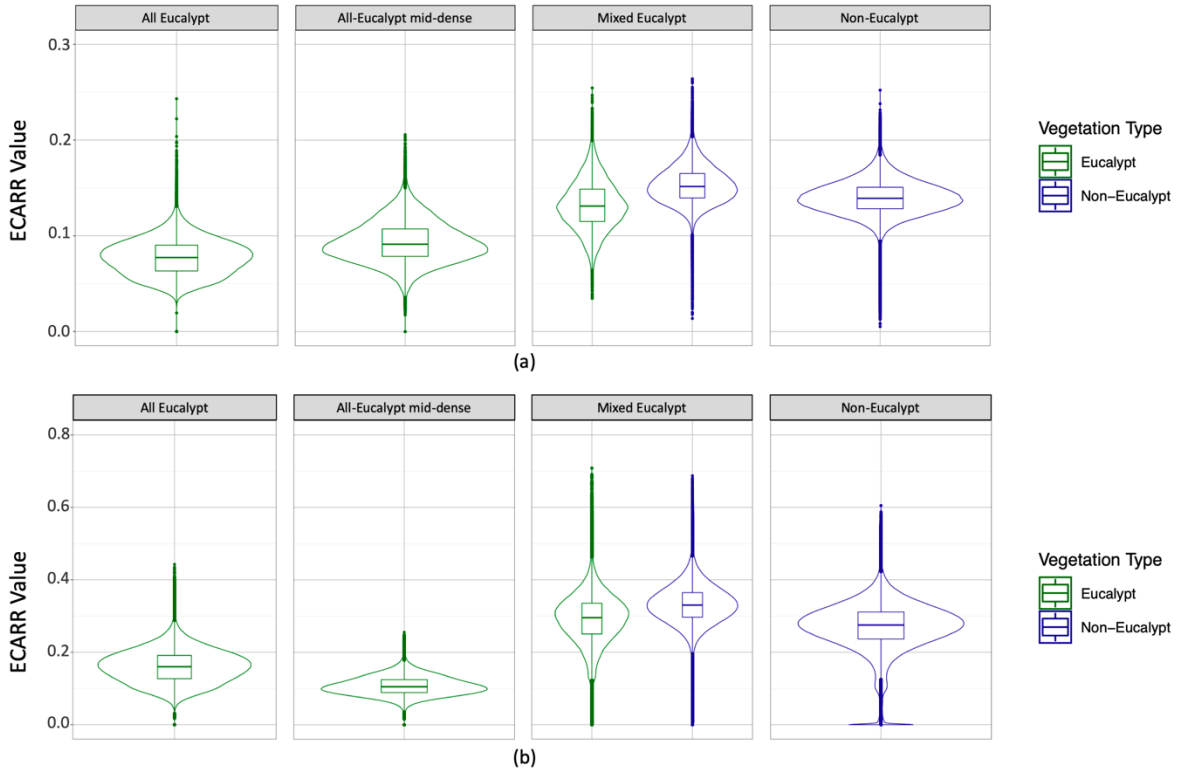

Figure 3. Violin box plots of ECARR values across sites and sensors by vegetation type. a) ECARR values from Sentinel-2 imagery at all sites. b) ECARR values from Planet imagery at all sites. Plots shown with sensor-specific y-axes, see Figure S7 for plots with unified scale.

The distribution of ECARR values in the Sentinel-2 imagery and Planet imagery show consistent trends that non-eucalypt vegetation has higher ECARR values (Figure 4). When assessed by vegetation density structure according to the 2017 VMRE map, ECARR values are higher in areas with denser vegetation (Figure S8-S10) and ANOVA tests show values were significantly different between density types ($p = 0$) (Table S8, S10). The highest mean ECARR values in eucalypt vegetation were found in the mixed-eucalypt site. Spatially, these 'high' (>0.15) ECARR values of eucalypt vegetation cluster at the lower elevations near the bases of the Pelion State Forest hills and along boundaries with non-eucalypt vegetation communities (Figure S13).

ECARR values from the summer imagery analysis are consistent with the winter imagery (Figure S25-S28). The distribution of ECARR values between vegetation types showed an increase in separation in the Planet imagery (Figure S26), while Sentinel-2 imagery showed an increase in distribution overlap (Figure S25). The ranges across all sites and sensors were smaller than found in the winter imagery but similarly Planet imagery had higher ranges

Preprints (www.preprints.org) | NOT PEER-REVIEWED | Posted: 23 November 2020 doi:10.20944/preprints202011.0574.v1

and mean for all three large sites analyzed (Table S17). ECARR values in different density groups were also found to be significantly different from one another in ANOVA tests for both satellite types (Table S19, S21).

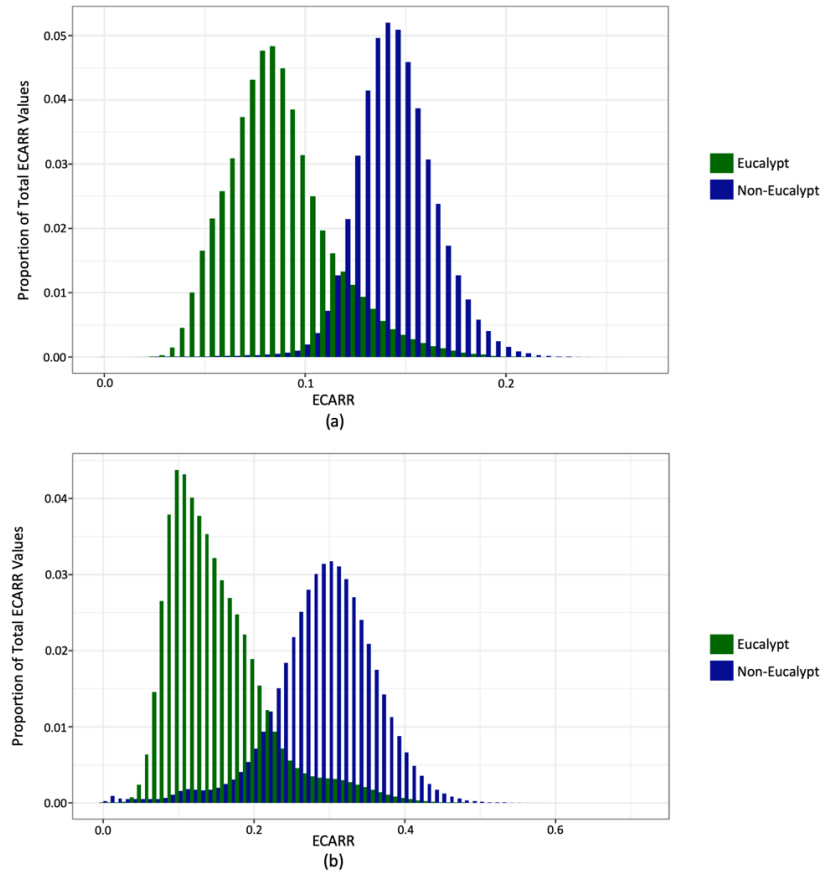

Figure 4. Proportion of ECARR values across all sites by vegetation type. a) Proportion of total ECARR values at all sites from Sentinel-2 imagery grouped by vegetation type. b) Proportion of total ECARR values at all sites from Planet imagery grouped by vegetation type.

ECBRR Results

ECBRR values ranged between 0 and 0.1 across all sites and sensors (Table 5). The range of ECBRR values was greater in the Sentinel-2 imagery than the Planet imagery, with the highest mean value found in the mixed eucalypt site and lowest mean value found in the large all-eucalypt site (Figure 5, Table 5). The ECBRR value ranges in the mid-dense all-eucalypt and non-eucalypt sites were similar between satellites, but the mixed eucalypt site showed the greatest change in range between sensors. ECBRR can identify mid-dense eucalypt vegetation (Figure 5a) in the all-eucalypt sites but it also falsely identified eucalypt vegetation in non-eucalypt vegetation communities (Figure 5d,h) with higher values on average (Table 5, Figure 6).

Preprints (www.preprints.org) | NOT PEER-REVIEWED | Posted: 23 November 2020 doi:10.20944/preprints202011.0574.v1

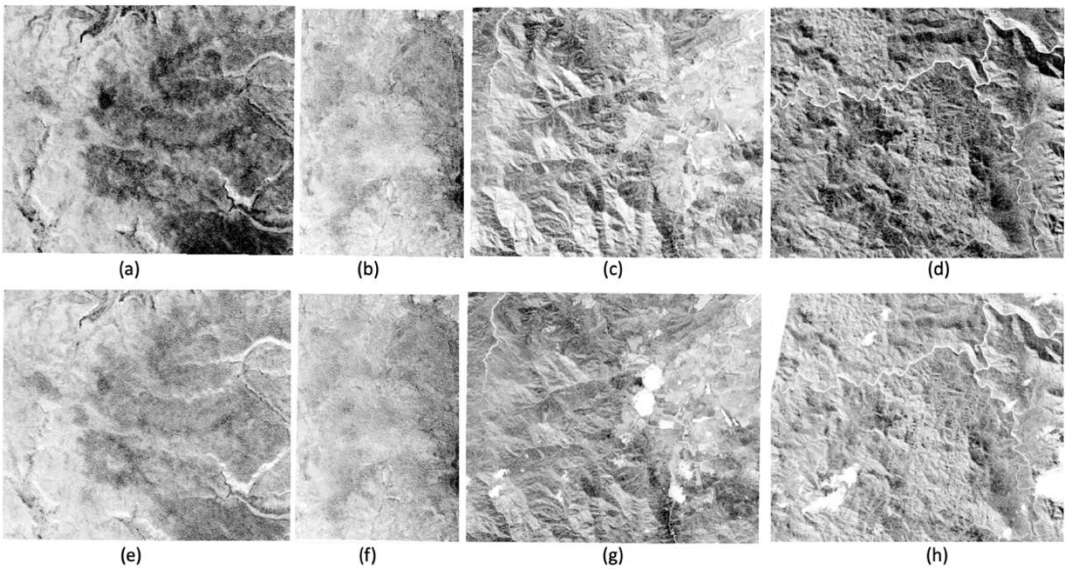

Figure 5. Results of Eucalypt Chlorophyll-*b* Reflectance Ratio (ECBRR) calculations shown with a gradient color scale from white (low) to black (high). Panels a-d) show Sentinel-2 imagery. Panels e-h) show Planet imagery. a) All-eucalypt site ECBRR results Sentinel-2A imagery. b) All-eucalypt mid-dense site ECBRR results Sentinel-2B imagery. c) Mixed eucalypt site ECBRR results Sentinel-2A imagery. d) Non-eucalypt site ECBRR results Sentinel-2B imagery. e) All-eucalypt site ECBRR results Planet imagery. f) All-eucalypt mid-dense site ECBRR results Planet imagery. g) Mixed eucalypt site ECBRR results Planet imagery. h) Non-Eucalypt site ECBRR results Planet imagery.

Table 5. Eucalypt Chlorophyll-*b* Reflectance Ratio value ranges for all sites and satellite sensors from winter imagery.

Satellite	ECBRR Value	Large All-Eucalypt Site	All- Eucalypt Mid-dense Site	Mixed Eucalypt Site	Non-Eucalypt Site
Sentinel-2	Maximum	0.022	0.019	0.085	0.056
	Minimum	0.000	0.000	0.000	0.000
	Mean	0.002	0.003	0.013	0.009
Planet	Maximum	0.021	0.012	0.050	0.055
	Minimum	0.000	0.000	0.000	0.000
	Mean	0.002	0.002	0.007	0.007

Consistent with ECARR, ROC curves for ECBRRs ability to classify eucalypt vegetation across sensors show the Sentinel-2 instrument (AUC: 0.893, Accuracy: 0.855, PPV: 0.868, NPV: 0.841) had higher accuracy than the Planet Dove (AUC: 0.877, PPV: 0. 868, NPV: 0.841) (Figure S15, S16, Table S11, S12). Density structure impacted ECBRR values (Figure S17-S19) and ANOVA tests show density groups were significantly different from each other (Tables S14, S16). The highest mean ECBRR value in eucalypt vegetation was likewise found in the mixed-eucalypt site (Table 5). High ECBRR values are also spatially clustered in areas of lower elevations near the base of the Pelion State Forest hills (Figure S22).

Preprints (www.preprints.org) | NOT PEER-REVIEWED | Posted: 23 November 2020 doi:10.20944/preprints202011.0574.v1

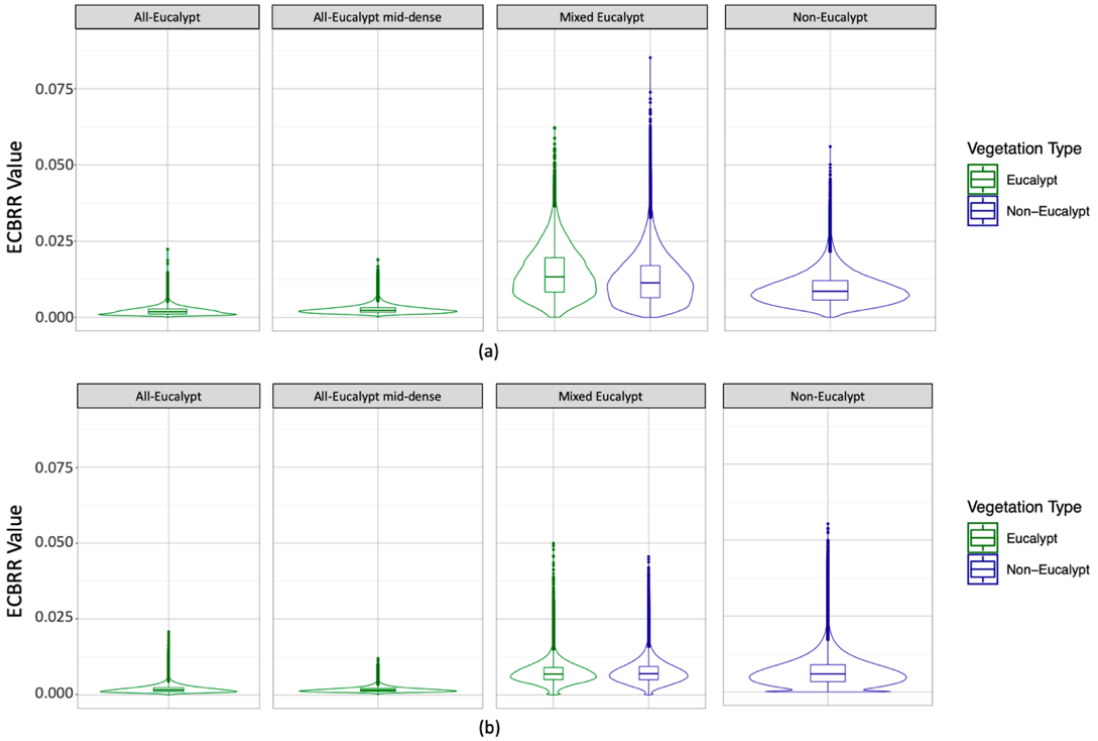

Figure 6. Violin Box plots of ECBRR values across sites and sensors. a) ECBRR values from Sentinel-2 imagery at all sites. b) ECBRR values from Planet imagery at all sites.

The distribution of ECBRR was not significantly impacted by site (Figure S20-S21), shown by the substantial overlap of the non-eucalypt and mixed eucalypt site value distributions across both satellite types. Regardless of vegetation attribute, there is little separation between maximum and minimum values across all sites, sensors, and seasons.

ECBRR values from the summer imagery analysis were also comparable with the winter analysis. Areas of non-eucalypt vegetation were found to have higher mean ECBRR values than eucalypt vegetation (Figure S29, S30, Table S22). Planet imagery showed increased separation in ECBRR distributions between vegetation types (Figure S30), while Sentinel-2 imagery showed an increase in ECBRR's distribution overlap (Figure S29). The ranges across all sites were similar to those found in the winter imagery. The non-eucalypt site in the Sentinel-2 image had the highest range and mean for all large sites (Table S22) and density groups were significantly different from each other (Table S24, S26).

Preprints (www.preprints.org) | NOT PEER-REVIEWED | Posted: 23 November 2020 doi:10.20944/preprints202011.0574.v1

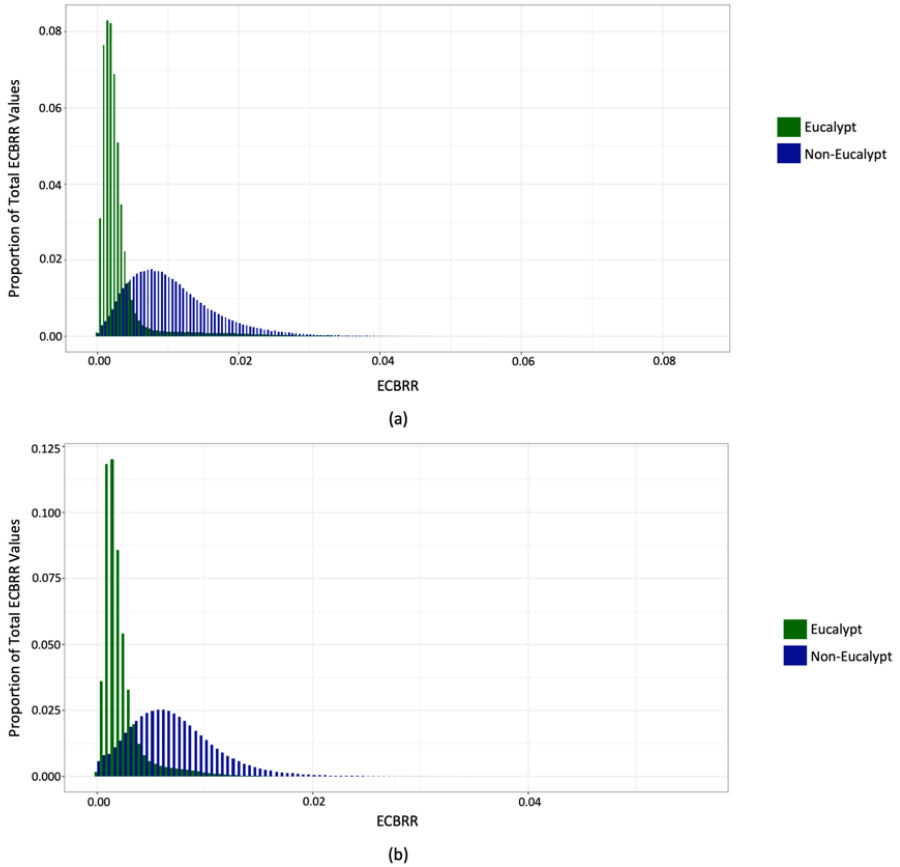

Figure 7. Proportion of ECBRR values across all sites by vegetation type. a) Proportion of total ECBRR values at all sites from Sentinel-2 imagery grouped by vegetation type. b) Proportion of total ECBRR values at all sites from Planet imagery grouped by vegetation type.

NDVI Results

All four sites had relatively high NDVI values in the Planet and Sentinel-2 imagery (Table 6, Figure S23), showing each site contained areas of green, healthy vegetation. In both types of imagery, the large all-eucalypt site had the lowest maximum and mean NDVI value as compared to the other sites. The mixed eucalypt site and non-eucalypt site showed relatively consistent NDVI values across all vegetated areas regardless of vegetation density (Figure S24). Little difference in NDVI ranges and means were seen between vegetation types in the mixed eucalypt site (Figure S23). Overall, the two all-eucalypt sites had the lowest mean NDVI values of all sites analyzed. Late spring/summer results show similar trends to winter with all sites having lower maximum values and means, except for the non-eucalypt site which had nearly equivalent means for both sensors. The relationship between NDVI and ECARR values for each site is shown in Figure 9.

 doi:10.20944/preprints202011.0574.v1

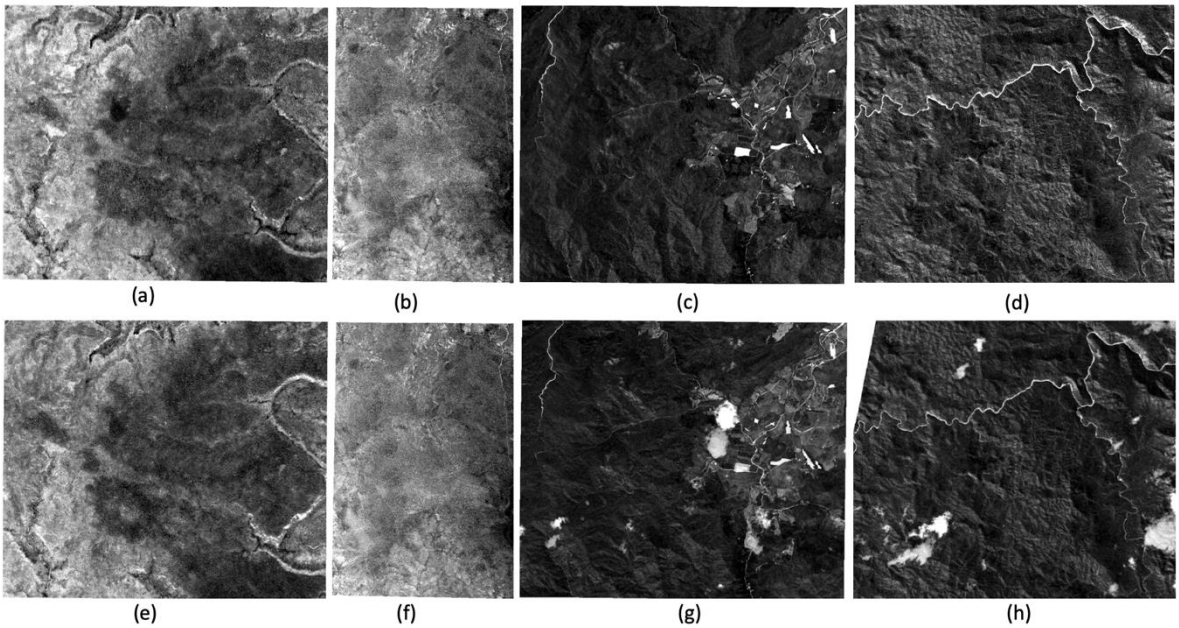

Figure 8. Results of Normalized Difference Vegetation Index (NDVI) calculations shown with a gradient color scale from white (low) to black (high). Panels a-d) show Sentinel-2 imagery. Panels e-h) show Planet imagery. a) All-eucalypt site NDVI results Sentinel-2A imagery. b) All-eucalypt mid-dense site NDVI results Sentinel-2B imagery. c) Mixed eucalypt site NDVI results Sentinel-2A imagery. d) Non-eucalypt site NDVI results Sentinel-2B imagery. e) All-eucalypt site NDVI results Planet imagery. f) All-eucalypt mid-dense site NDVI results Planet imagery. g) Mixed eucalypt site ECARR results Planet imagery. h) Non-Eucalypt site NDVI results Planet imagery.

Table 6. NDVI value ranges for all sites and satellite sensors from winter imagery.

Satellite	NDVI Value	Large All-Eucalypt Site	All-Eucalypt Mid-dense Site	Mixed Eucalypt Site	Non-Eucalypt Site
Sentinel-2	Maximum	0.801	0.789	0.844	0.843
	Minimum	-0.041	0.185	0.047	-0.035
	Mean	0.513	0.559	0.738	0.719
Planet	Maximum	0.830	0.752	0.873	0.867
	Minimum	0.157	0.208	0.005	-0.101
	Mean	0.600	0.549	0.754	0.727

Preprints (www.preprints.org) | NOT PEER-REVIEWED | Posted: 23 November 2020 doi:10.20944/preprints202011.0574.v1

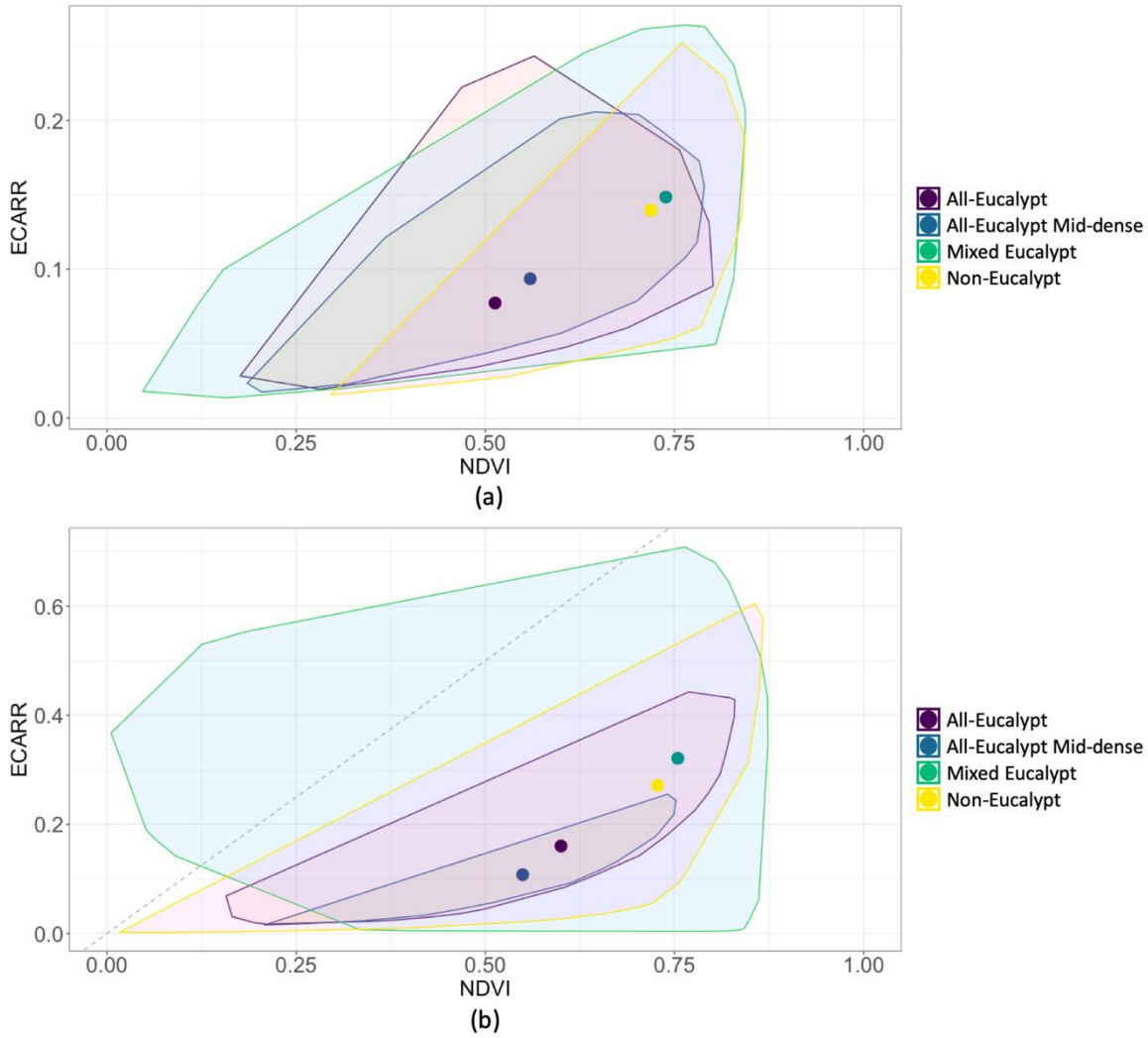

Figure 9. Mean ECARR values and mean NDVI values at all sites in winter imagery with convex hulls of values as polygons. a) Mean ECARR and NDVI values (points) with a convex hull represented by polygons from Sentinel-2 winter imagery at all sites and grey dashed 1-to-1 line. b) Mean ECARR and NDVI values (points) with a convex hull represented by polygons from Planet winter imagery at all sites and grey dashed 1-to-1 line.

4. Discussion

Eucalypt Chlorophyll-a Reflectance Ratio (ECARR)

Eucalypt vegetation was correctly identified in both all-eucalypt sites and the mixed eucalypt site (Figure 3, 4). Planet imagery had consistently higher ECARR values than the Sentinel-2 imagery, likely due to the higher resolution of the image. This increased resolution likely lends power to ECARR's ability to detect chlorophyll properties by reducing the variation of vegetation within a single pixel, therefore increasing the granularity of the vegetation's reflectance signal. The highest ECARR values within the all-eucalypt site were found in the sparsely vegetated areas dominated by *C. citriodora* open forests. Similar to the location of the 'high' ECARR and ECBRR values in the mixed-eucalypt site, this pixel was at the base of a ridge. These soils may have higher water content from

drainage down the hillside and vegetation grows better here, thus reflecting more chlorophyll and increasing ECARR values. Both satellites showed they were capable of identifying eucalypts with a mid-dense canopy structure, but struggled to highlight sparser vegetation in surrounding areas (Figure 2a, 2d). The areas of low ECARR values (Figure 2a) correspond with areas of lower NDVI values (Figure 6a), suggesting that there is less chlorophyll reflectance from any type of vegetation in these pixels, relative to surrounding areas. Mean ECARR values from the Sentinel-2 large all-eucalypt site increased when pixels were selected for high NDVI values (>0.5) (Figure S14). ECARR values also increased with increasing density of the vegetation canopy (Figure S8, S9) and different density groups were significantly different from one another in ANOVA tests. This validates that canopy density substantially influences the ability of ECARR to identify eucalypt vegetation remotely. The late spring/summer imagery ECARR analysis echoes these trends but with slightly smaller ranges and lower means for the three large sites analyzed across both sensors. This could be due to the vegetation putting more energy into reproduction rather than growth during this time or biotic factors that impacted growth during these months. The spring of 2019 was the driest and the second warmest on record for Australia [28]. The decrease in ranges and means of ECARR at all sites likely show the effect of these extreme environmental conditions.

The mixed eucalypt site (Figure 2c, 2g) contained the greatest ECARR value calculated across all sites and sensors (Table 4.) It was calculated in an area of mid-dense vegetation consisting of *E. resinifera* and/or *E. portuensis (*Figure S7b). Interestingly, the agricultural fields in both types of imagery had low ECARR values (Figure 2c, 2g), suggesting this reflectance ratio may be able to discern native vegetation chlorophylls from cultivated crop chlorophylls. The scene still contained relatively high ECARR values in areas of both eucalypt and non-eucalypt vegetation (Figure 3), but high values in the eucalypt vegetation communities were spatially clustered in areas of lower elevation (Figure S13) where vegetation likely benefits from the water drainage down these slopes. Other high eucalypt ECARR values were along boundaries between eucalypt and non-eucalypt vegetation communities (Figure 2c), which could reflect differences in vegetation boundaries between the VMRE maps and the landscape.

Mean ECARR values in the non-eucalypt site were higher than both all-eucalypt sites in both sensor types (Table 4, Figure 3). Surprisingly, ECARR values did not differ greatly between density structures; both ‘dense’ and ‘very sparse’ vegetation showed similar mean values (Figure S8). However, the ‘very sparse’ vegetation is very small in geographic extent (<0.05% of pixels) and is surrounded by dense vegetation. It’s possible the satellite resolutions were too coarse to distinguish this very small area of sparse vegetation from its surroundings. There could also be boundary discrepancies between the VMRE map and the landscape which could have allowed for ‘dense’ vegetation on the landscape to be classified in the ‘very sparse’ area from the VMRE map.

ROC curves for each satellite show that ECARR was sensitive enough to identify eucalypt vegetation and had higher sensitivity, negative predictive power, and positive predictive power in the Sentinel-2 imagery. This is likely due to the closer band match of this sensor’s spectral bands to the original reflectance ratio. The center wavelength of Sentinel-2’s band 5 is only 5nm off from the original reflectance ratio, while Planet’s corresponding band was 40nm off. Both satellites also show ECARR has low specificity when discerning eucalypt

 doi:10.20944/preprints202011.0574.v1

vegetation from other vegetation types. This is corroborated by the higher mean ECARR values in the non-eucalypt site than the large and mid-dense all-eucalypt sites for both satellites (Figure 3) and seasons (Figure S25, S26). These results demonstrate that satellite-derived ECARR values are not specific enough to discriminate between eucalypt and non-eucalypt types of vegetation.

Eucalypt Chlorophyll-b Reflectance Ratio (ECBRR)

ECBRR results show similar trends to ECARR across sites and seasons but values were an order of magnitude smaller than ECARR and NDVI. The lowest maximum and mean ECBRR values for both satellite types were found in the large all-eucalypt and mid-dense eucalypt site (Table 5). Unlike ECARR, the greatest ECBRR values were detected in Sentinel-2 imagery. However, the ranges and means of ECBRR values are very narrow, making it difficult to say with confidence whether this algorithm can discern vegetation from non-vegetation remotely.

The mixed eucalypt site similarly contained pixels with the highest ECBRR values near the slopes of the Pelion State Forest hills and along boundaries between vegetation communities. However, the agricultural fields that were readily distinguished by ECARR (Figure 2c,g), are not as easily discernable and blend in with the nearby forest due to their similarly low ECBRR values. This implies that ECBRR cannot distinguish between chlorophyll reflectance of native vegetation and cultivated crops. The non-eucalypt site contained higher maximum values of ECBRR in both types of satellite imagery than the large all-eucalypt site. Although ROC curves indicated that ECBRR was sensitive enough to identify eucalypt vegetation in both types of imagery (Figure S15, S16), the very low means and narrow ranges of ECBRR suggest other spectral indices, such as ECARR or NDVI, are better at identifying vegetation remotely and offer more separation in values between vegetation and non-vegetation in satellite imagery.

Normalized Difference Vegetation Index (NDVI)

The substantial overlap of ECARR and NDVI value ranges across sites (Figure 9) further supports that ECARR is sufficiently sensitive to identify vegetation, but it cannot distinguish between vegetation types. However, NDVI values (Figure 6c, 6g) were relatively high and consistent between the agricultural fields and the neighboring dense forest. This further promotes that ECARR may emphasize reflective differences between chlorophylls in native vegetation and cultivated crops. We believe the high sensitivity but low specificity in ECARR's ability to identify eucalypt vegetation is due to differences in the wide range of spectral wavelengths collected by these sensors and the original algorithm. The lack of specificity and low values from high-resolution imagery (3-20m) suggests ECARR should not be used on the satellite data sources considered here to assess changes in eucalypt vegetation dynamics or biodiversity over time with confidence. ECBRR is also not readily applicable to identify eucalypt vegetation remotely with high confidence from the satellite imagery assessed here. The algorithms alone, when applied to either source of imagery, do not provide enough information to classify eucalypt vegetation extent.

There are several factors in this study that may have impacted ECARR and ECBRR results at the sites tested. When developing these ratios, the correlation factor rapidly declines just a few wavelengths around the peak wavelengths of 550nm, 708nm, and 860nm [14], so it is likely the bands in the imagery used here were too far from the original bands to reprise

 doi:10.20944/preprints202011.0574.v1

those results. Additional errors could be due to the characteristics of the vegetation communities selected. Large areas of or monogenus or monotribe eucalypt vegetation on the Vegetation Management Regional Ecosystem maps are rare in Queensland. Australia has lost nearly 40% of its forest since European colonization in roughly 1750 and areas of native forest have become increasingly fragmented over time [29]. No 'dense' eucalypt vegetation patches are present on the 2017 VMRE map, so a comparison of 'dense' eucalypt and non-eucalypt areas was not possible. The large all-eucalypt site, which was the only area of its size found on the 2017 VMRE map, contained mostly areas of sparse vegetation. We see this had a direct negative impact on ECARR, ECBRR, and NDVI values from this site (Figure 2,4,6).

Abiotic factors such as topography, elevation, average rainfall, and temperature also impact vegetation communities broadly. Rapid decreases in elevation spatially correlated with higher ECARR and ECBRR values in the mixed-eucalypt site. It's likely that other environmental factors not considered here also influenced the distribution of ECARR values at each site. Biotic factors such as eucalypt physiology and spatial canopy structure may have also limited the ability to measure eucalypt chlorophylls from satellite imagery. Eucalypts have pendular leaf morphology [14,30], causing the leaves to hang downward, which can impact the appearance of eucalypt canopy density from above-ground imagery. Lastly, as shown in previous work, some individual species were shown to have higher correlations with a modified index [15] than when it was applied to areas of mixed species. It is possible the diversity of *Eucalyptus* species at these sites gave lower correlations with ECARR and ECBRR than if these *Eucalyptus* species were evaluated individually.

Further studies need to be done to test the use of ECARR and ECBRR on remotely collected data. These analyses should be repeated on smaller sites with uniform vegetation types and elevations to test the effect of canopy structure on ECARR more closely. Similarly, these could be repeated on areas of single species to categorize ECARR ranges for different eucalypt species. Additionally, high-resolution multispectral imagery with very narrow ranges of spectral bands may be able to remotely measure chlorophyll-*a* better than sensors with wide ranges of spectral bands. This could reveal new or improved correlations at different wavelengths captured by satellites and may lead to the development of a version of ECARR better suited for satellite imagery.

While the eucalypt chlorophyll reflectance ratios tested here were not able to distinguish the eucalypt tribe of vegetation from other types on previously collected imagery, the incredibly detailed VMRE maps can still benefit from newly-available, high-resolution, globally-comprehensive satellite imagery. These increasingly powerful sensors can help to assess plant presence and absence, and chlorophyll properties at finer spatial scales. We can assess vegetation losses in greater detail now than ever before and can apply these tools to inform reactive conservation and preservation policy as necessary on rapidly changing landscapes or in a changing climate. It is crucial to develop and refine our vegetation classification tools on satellite imagery so we know how vegetation communities and biodiversity are being impacted in areas where no vegetation mapping products exist.

 doi:10.20944/preprints202011.0574.v1

5. Conclusions

When applied to passively collected imagery of landscapes from Sentinel-2 and Planet, and likely other sources as well, Eucalypt Chlorophyll-*a* Reflective Ratio can serve as a general chlorophyll indicator but is not a specific index with which to identify *Eucalyptus* vegetation with certainty. This is likely due to the large range of wavelengths collected by the sensors and imperfect band matches to the original algorithm. Eucalypt Chlorophyll-*b* Reflective Ratio values were an order of magnitude smaller than ECARR and NDVI and should be used with caution when evaluating vegetation chlorophyll properties from satellite imagery. Further studies need to be done to reassess the correlations between eucalypt chlorophyll-*a* and eucalypt chlorophyll-*b* and the wide ranges of wavelengths collected from the many passive satellites currently imaging the globe. With improved calibrations of these reflectance ratios, it may be possible to leverage previously collected satellite imagery to classify eucalypt distribution in areas with no existing information on vegetation communities.

Supplementary Materials: The following are available online at *www.mdpi.com/xxx/s1*,
Figure S1: All-eucalypt site from the 2017 VMRE map colored by vegetation type where green represents areas dominated by eucalypt vegetation.
Figure S2: All-eucalypt mid-dense site from the 2017 VMRE map colored by vegetation type where green represents areas dominated by eucalypt vegetation.
Figure S3: Mixed eucalypt site from the 2017 VMRE map colored by vegetation type where green represents areas dominated by eucalypt vegetation, blue represents areas dominated by non-eucalypt vegetation, and grey represents non-remnant areas (cleared land).
Figure S4: Non-eucalypt site from the 2017 VMRE map colored by vegetation type where blue represents areas dominated by non-eucalypt vegetation.
Figure S5: ROC Curve for ECARR's ability to detect eucalypt vegetation from Sentinel-2 winter imagery.
Figure S6: ROC Curve for ECARR's ability to detect eucalypt vegetation from Planet winter imagery.
Figure S7: Violin box plots of ECARR values in winter imagery across sites and sensors by vegetation type as characterized in the 2017 VMRE map with unified scale.
Figure S8: Violin box plots of ECARR values in winter imagery across sites and sensors by vegetation type and vegetation density as characterized in the 2017 VMRE map.
Figure S9: Sentinel-2 winter imagery ECARR value distribution across all sites colored by density structure.
Figure S10: Planet winter imagery ECARR value distribution across all sites colored by density structure.
Figure S11: Sentinel-2 winter imagery ECARR value distribution across all sites colored by site.
Figure S12: Planet winter imagery ECARR value distribution across all sites colored by site.
Figure S13: Mixed Eucalypt Site with Digital Elevation Model colorized with white as high elevation and black as low elevation and high ECARR values in eucalypt vegetation communities in green from winter imagery.

 doi:10.20944/preprints202011.0574.v1

 doi:10.20944/preprints202011.0574.v1

Table S4: Description of non-eucalypt site vegetation communities from the 2017 VMRE map.
Table S5: Sentinel-2 ECARR ROC curve specificity and sensitivity for ECARR with 'best' method.
Table S6: Planet ECARR ROC curve specificity and sensitivity for ECARR with 'best' method.
Table S7: ANOVA Table (type II tests) for effect of vegetation type on ECARR for Sentinel-2 winter imagery.
Table S8: ANOVA Table (type II tests) for effect of density structure on ECARR for Sentinel-2 winter imagery.
Table S9: ANOVA Table (type II tests) for effect of vegetation type on ECARR for Planet winter imagery.
Table S10: ANOVA Table (type II tests) for effect of density structure on ECARR for Planet winter imagery.
Table S11: Sentinel 2 ECBRR ROC curve specificity and sensitivity for ECBRR on winter imagery with 'best' method.
Table S12: Planet ECBRR ROC curve specificity and sensitivity for ECBRR on winter imagery with 'best' method.
Table S13: ANOVA Table (type II tests) for effect of vegetation type on ECBRR for Sentinel-2 winter imagery.
Table S14: ANOVA Table (type II tests) for effect of density structure on ECBRR for Sentinel-2 winter imagery.
Table S15: ANOVA Table (type II tests) for effect of vegetation type on ECBRR for Planet winter imagery.
Table S16: ANOVA Table (type II tests) for effect of density structure on ECBRR for Planet winter imagery.
Table S17: Eucalypt Chlorophyll-a Reflectance Ratio value ranges and mean of late spring/summer imagery for the three large sites and both satellite sensors.
Table S18: ANOVA Table (type II tests) for vegetation type on ECARR for Sentinel-2 late spring/summer imagery.
Table S19: ANOVA Table (type II tests) for effect of density structure on ECARR for Sentinel-2 late spring/summer imagery.
Table S20: ANOVA Table (type II tests) for vegetation type on ECARR for Planet late spring/summer imagery.
Table S21: ANOVA Table (type II tests) for effect of density structure on ECARR for Planet late spring/summer imagery.
Table S22: ANOVA Table (type II tests) for vegetation type on ECARR for Sentinel-2 late spring/summer imagery.
Table S23: ANOVA Table (type II tests) for effect of density structure on ECARR for Sentinel-2 late spring/summer imagery.
Table S24: ANOVA Table (type II tests) for vegetation type on ECARR for Planet late spring/summer imagery.

Table S25: ANOVA Table (type II tests) for effect of density structure on ECARR for Planet late spring/summer imagery.
Table S26: Eucalypt Chlorophyll-b Reflectance Ratio value ranges and mean of late spring/summer imagery for the three large sites and both satellite sensors.
Table S27: Normalized Difference Vegetation Index value ranges and mean of late spring/summer imagery for the three large sites and both satellite sensors.

Author Contributions: Conceptualization, T.T., N.B., and K.B.; methodology, K.B., T.T., N.B., and B.L.; software, K.B., T.T., and B.L.; validation, K.B., and T.T.; formal analysis, K.B. and T.T.; investigation, K.B., and T.T.; resources, K.B., T.T., and N.B.; data curation, K.B., and T.T.; writing—original draft preparation, K.B.; writing—review and editing, K.B., N.B., T.T.; visualization, K.B.; supervision, N.B.; project administration, N.B.; funding acquisition, N.B., K.B, and T.T. All authors have read and agreed to the published version of the manuscript.

Funding: This work was funded by the National Science Foundation (grant nos. CNH-L: 1716698 & GRFP: DGE1255832), the Defense Advanced Research Projects Agency PREEMPT program (Cooperative Agreement #D18AC00031), and The McNair Scholars Program at The Pennsylvania State University. The content of the information does not necessarily reflect the position or the policy of the U.S. government, and no official endorsement should be inferred.

Conflicts of Interest: The authors declare no conflict of interest. The funders had no role in the design of the study; in the collection, analyses, or interpretation of data; in the writing of the manuscript, or in the decision to publish the results.

References

1. Díaz, S.; Fargione, J.; Chapin, F.S.; Tilman, D. Biodiversity loss threatens human well-being. *PLoS Biol.* **2006**, *4*, 1300–1305, doi:10.1371/journal.pbio.0040277.

2. Chapin, F.S.; Zavaleta, E.S.; Eviner, V.T.; Naylor, R.L.; Vitousek, P.M.; Reynolds, H.L.; Hooper, D.U.; Lavorel, S.; Sala, O.E.; Hobbie, S.E.; et al. Consequences of changing biodiversity. *Nature* **2000**, *405*, 234–242, doi:10.1038/35012241.

3. Gamfeldt, L., Hillebrand, H., Jonsson, P.R. Multiple Functions Increase The Importance of Biodiversity for Overall Ecosystem Functioning. *Ecology* **2008**, *89*, 1223–1231.

4. Sturrock, R.N.; Frankel, S.J.; Brown, A. V.; Hennon, P.E.; Kliejunas, J.T.; Lewis, K.J.; Worrall, J.J.; Woods, A.J. Climate change and forest diseases. *Plant Pathol.* **2011**, *60*, 133–149, doi:10.1111/j.1365-3059.2010.02406.x.

5. Chornesky, E.A.; Bartuska, A.M.; Aplet, G.H.; Britton, K.O.; Cummings-Carlson, J.; Davis, F.W.; Eskow, J.; Grodon, D.R.; Gottschalk, K.W.; Haack, R.A.; et al. Science Priorities for Reducing the Threat of Invasive Species to Sustainable Forestry.

Bioscience **2005**, *55*, 335, doi:10.1641/0006-3568(2005)055[0335:spfrtt]2.0.co;2.

6. Cahill, A.E.; Aiello-Lammens, M.E.; Caitlin Fisher-Reid, M.; Hua, X.; Karanewsky, C.J.; Ryu, H.Y.; Sbeglia, G.C.; Spagnolo, F.; Waldron, J.B.; Wiens, J.J. Causes of warm-edge range limits: systematic review, proximate factors and implications for climate change. *J. Biogeogr.* **2014**, *41*, 429–442, doi:10.1111/jbi.12231.

7. Pecl, G.T.; Araújo, M.B.; Bell, J.D.; Blanchard, J.; Bonebrake, T.C.; Chen, I.-C.; Clark, T.D.; Colwell, R.K.; Danielsen, F.; Evengård, B.; et al. Biodiversity redistribution under climate change: {Impacts} on ecosystems and human well-being. *Science (80-.).* **2017**, *355*, eaai9214, doi:10.1126/science.aai9214.

8. Brook, B.W.; O'Grady, J.J.; Chapman, A.P.; Burgman, M.A.; Resit Akçakaya, H.; Frankham, R. Predictive accuracy of population viability analysis in conservation biology. *Nature* **2000**, *404*, 385–387, doi:10.1038/35006050.

9. Ehrlén, J.; Morris, W.F. Predicting changes in the distribution and abundance of species under environmental change. *Ecol. Lett.* **2015**, *18*, 303–314, doi:10.1111/ele.12410.

10. Queensland Herbarium Regional Ecosystem Description Database (REDD). Version 11.1 (April 2019). *Queensl. Dep. Environ. Sci. Brisbane* **2019**.

11. V.J. Neldner, B.A. Wilson, H.A. Dillewaard, T.S. Ryan, D.W. Butler, W.J.F. McDonald, E.P.A. and C.N.A. Methodology for survey and mapping of regional ecosystems and vegetation communities in Queensland.Version 5.0. Updated March 2019. *Queensl. Herb. Queensl. Dep. Environ. Sci. Brisbane.* **2019**.

12. Herold, M.; Mayaux, P.; Woodcock, C.E.; Baccini, A.; Schmullius, C. Some challenges in global land cover mapping: {An} assessment of agreement and accuracy in existing 1 km datasets. *Remote Sens. Environ.* **2008**, *112*, 2538–2556, doi:10.1016/j.rse.2007.11.013.

13. NASA Normalized Difference Vegetation Index (NDVI) Available online: https://earthobservatory.nasa.gov/features/MeasuringVegetation/measuring_vegetation_2.php (accessed on Dec 20, 2019).

14. Datt, B. Remote sensing of chlorophyll a, chlorophyll b, chlorophyll a+b, and total carotenoid content in eucalyptus leaves. *Remote Sens. Environ.* **1998**, *66*, 111–121, doi:10.1016/S0034-4257(98)00046-7.

15. Coops, N.C.; Stone, C.; Culvenor, D.S.; Chisholm, L.A.; Merton, R.N. Chlorophyll content in eucalypt vegetation at the leaf and canopy scales as derived from high

resolution spectral data. *Tree Physiol.* **2003**, *23*, 23–31, doi:10.1093/treephys/23.1.23.

16. Giles, J.R.; Plowright, R.K.; Peel, A.J.; Eby, P.; McCallum, H. Models of Eucalypt phenology predict bat population flux. *Ecol. Evol.* **2016**, *6*, 7230–7245, doi:10.1002/ece3.2382.

17. Giles, J.R.; Eby, P.; Parry, H.; Peel, A.J.; Plowright, R.K.; Westcott, D.A.; McCallum, H. Environmental drivers of spatiotemporal foraging intensity in fruit bats and implications for Hendra virus ecology. *Sci. Rep.* **2018**, *8*, 9555, doi:10.1038/s41598-018-27859-3.

18. Datt, B. A new reflectance index for remote sensing of chlorophyll content in higher plants: Tests using Eucalyptus leaves. *J. Plant Physiol.* **1999**, *154*, 30–36, doi:10.1016/S0176-1617(99)80314-9.

19. Giles, J.R.; Plowright, R.K.; Peel, A.J.; Eby, P.; McCallum, H. Models of {Eucalypt} phenology predict bat population flux. *Ecol. Evol.* **2016**, *6*, 7230–7245, doi:10.1002/ece3.2382.

20. Laperra, Valero, Santos-Rodriguez, R. Spatial/Spectral Information Trade-off in Hyperspectral Images. *IEEE* **2015**, 1124–1127.

21. European Space Agency MultiSpetral Instrument (MSI) Overview Available online: https://sentinel.esa.int/web/sentinel/technical-guides/sentinel-2-msi/msi-instrument (accessed on Dec 21, 2019).

22. Planet Team Planet Application Program Interface: In Space for Life on Earth Available online: https://developers.planet.com/docs/data/ (accessed on Dec 22, 2019).

23. Planet Team Understanding PlanetScope Instruments Available online: https://developers.planet.com/docs/data/sensors/ (accessed on Dec 21, 2019).

24. USGS Earth Explorer Available online: https://earthexplorer.usgs.gov/ (accessed on Nov 2, 2019).

25. Planet Team Planet Explorer Available online: https://www.planet.com/explorer/ (accessed on Sep 22, 2019).

26. ESRI ArcGIS Pro, Version 2.5, 2020.

27. R Core Team R: A language and environment for statistical computing. R Foundation for Statistical Computing, 2019.

28. BOM Special Climate Statements 72 — dangerous bushfire weather in spring 2019. *Aust. Gov.* **2019**, 28.

29. Bradshaw, C.J.A. Little left to lose: Deforestation and forest degradation in Australia since European colonization. *J. Plant Ecol.* **2012**, *5*, 109–120, doi:10.1093/jpe/rtr038.

30. Greaves, B L., Spencer, R.D. An evaluation of spectroradiometry and multispectral scanning for differentiating forest communities. *Aust. For.* **1993**, *56*, 68–79.